

Hybrid Photon-magnon Systems: Exploring the Purcell Effect

Sachin Verma,¹ Abhishek Maurya,¹ Fizaan Khan,¹ Kuldeep Kumar Shrivastava,¹ Rajeev Singh,¹ and Biswanath Bhoi¹

*Nano-Magnetism and Quantum Technology Lab,
Department of Physics,
Indian Institute of Technology (Banaras Hindu University) Varanasi,
Varanasi - 221005,
BHARAT (India).*

(*Electronic mail: biswanath.phy@iitbhu.ac.in)

(Dated: 9 January 2025)

We present a novel approach to observing the Purcell effect in a photon-magnon coupled (PMC) hybrid system consisting of a yttrium iron garnet (YIG) thin film and a hexagonal ring resonator (HRR) arranged in a planar geometry. This hybrid system has been designed and simulated using the commercial electromagnetic full-wave simulator CST Microwave Studio for various values of damping constant (α) of the YIG film while keeping the HRR properties constant. Our results reveal that as the magnon damping increases, the anti-crossing behavior between photon and magnon modes in the transmission spectra diminishes, transitioning the coupled modes into the Purcell regime. This transition is attributed to an enhanced spontaneous emission rate of microwave photons when coupled to lossy magnons, driving the PMC system into the Purcell regime. To elucidate this behavior, we developed a comprehensive theoretical framework based on a quantum model, which accurately describes the observed Purcell phenomena and provides estimations of the PMC strength ($g/2\pi$). Notably, by tuning α from 1.4×10^{-5} to 2.8×10^{-2} , we achieved precise control over ($g/2\pi$) ranging from 63 MHz to 127 MHz. This study highlights the Purcell effect's role in enhancing photon decay rates and establish a clear relationship with PMC strength. Our work offers a comprehensive method for controlling photon resonance dissipation, opening new avenues for exploring the Purcell effect and its applications in on-chip functional devices leveraging magnon-photon interactions for quantum technologies.

I. INTRODUCTION

The interplay between light and matter underpins a wide range of phenomena in quantum optics and condensed matter physics, offering profound insights and enabling transformative applications in quantum information science and technology¹⁻⁶. Among these, the Purcell effect is a key concept that refers to an enhancement or suppression of spontaneous emission rates of a quantum source induced by its interaction with the environment⁷⁻¹⁵ (as shown in Fig. 1(a)). This phenomenon has been extensively investigated in photon-cavity systems, where the precise tuning of photon lifetimes by engineering the cavity's electromagnetic properties offers a compelling avenue for manipulating quantum states, with far-reaching implications in quantum information science, photonics, and materials engineering^{6,10,16-20}. While the Purcell effect has been studied using methods other than cavities, such as photonic crystals^{17,21-24}, whispering gallery modes^{17,25-27}, and one-dimensional photonic waveguides²⁸, its manifestation in hybrid systems involving coupled magnons and photons remains relatively unexplored.

Magnons, the quanta of spin waves, are known for their long coherence times and their ability to interact with various quantum platforms²⁹⁻³². The interaction between magnons and photons in hybrid quantum systems^{1,2,32-35} has attracted considerable attention in recent years, opening new avenues for exploring fundamental quantum phenomena and developing innovative devices^{1,2,4,26,34,36? -38}. In this context, demonstrating the Purcell effect in a photon-magnon coupled (PMC) system represents a significant advancement in leveraging magnonic platforms for quantum technologies.

In this work, we investigate the observation of the Purcell effect in a photon-magnon coupled hybrid system through numerical simulations, complemented by a quantum theoretical model. Unlike conventional approaches that rely on modifying cavity properties, we focus on a unique approach: we show that varying the intrinsic damping constant of the magnon mode offers a powerful means to induce and control the Purcell effect. By engineering the magnon damping, we achieve precise control over the hybridized mode lifetimes and their spectral characteristics. The quantum model offers a deeper understanding of the underlying mechanisms, validating the numerical findings and highlighting the conditions for optimizing the Purcell effect in these systems. The results not only extend the paradigm of cavity magnonics but also underscore the versatility of hybrid systems in addressing challenges in quantum technology.

II. NUMERICAL SIMULATION DETAILS

In order to explore the magnon dissipation-induced Purcell effect, we design a PMC hybrid system consisting of a hexagonal ring resonator (HRR) and a yttrium iron garnet (YIG) thin film in a planar geometry as schematically shown in Figure 1(b). The electromagnetic full-wave solver CST Microwave Studio was employed to conduct simulation and examine the dynamics of interaction between the YIG's magnon mode and HRR's photon mode. For microwave excitations in both the HRR and the YIG film, a microstrip feeding line was placed on the front side while the ground plane was on the back side of the sample. The dimensions of the HRR, the

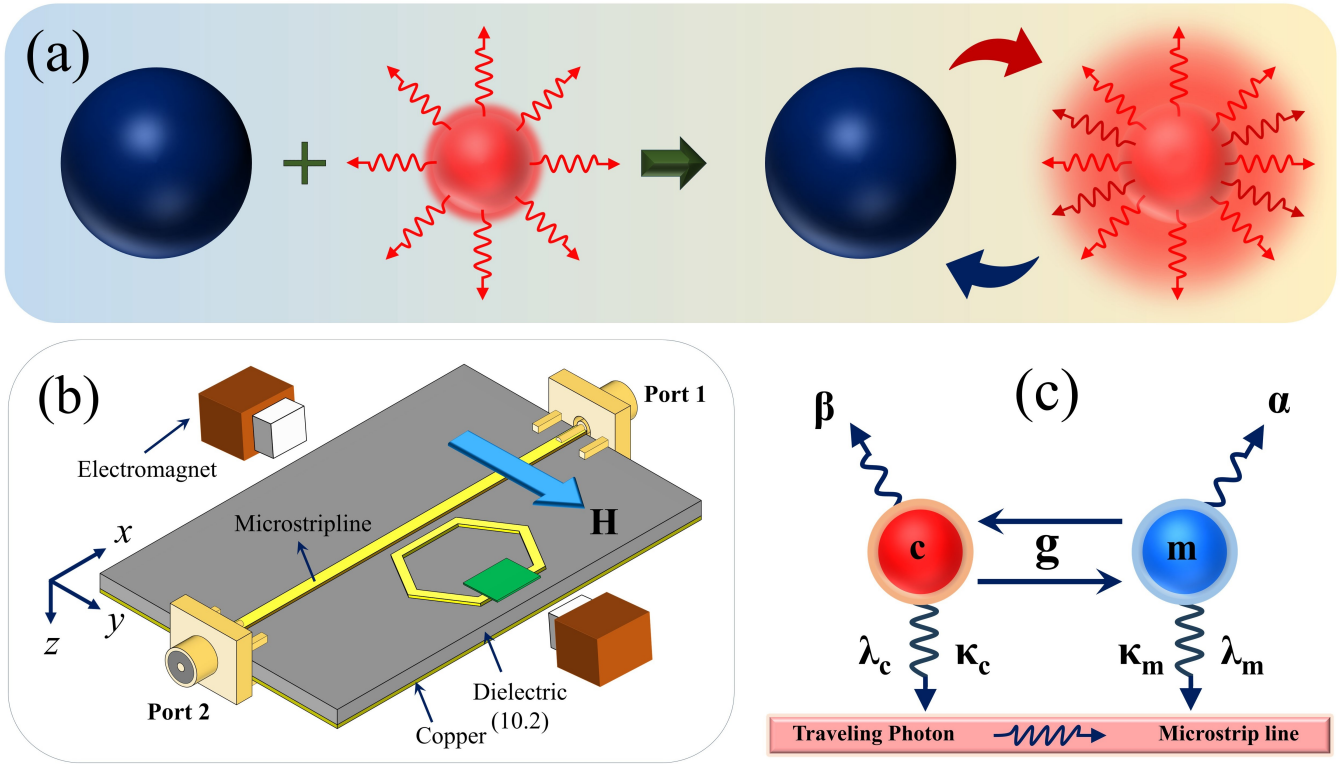


FIG. 1. (a) Schematic diagram of the Purcell effect, illustrating the enhancement of the spontaneous emission rate of the quantum source mediated by the atom-field interaction. (b) Simulation setup consisting of a YIG film (green) with dimensions $3\text{ mm} \times 3\text{ mm} \times 20\text{ }\mu\text{m}$, a microstrip line (dark yellow) with dimensions $30\text{ mm} \times 0.57\text{ mm} \times 35\text{ }\mu\text{m}$, a dielectric material (gray) with dimensions $30\text{ mm} \times 20\text{ mm} \times 0.64\text{ mm}$, and an HRR (with $a = 4\text{ mm}$, $b = 3.4\text{ mm}$) positioned near the microstrip line. (c) Schematic of the complex photon-magnon coupled hybrid system.

microstrip line, and the YIG film are indicated in the captions of Fig. 1 (b) (for further details, see Ref.³²).

For strong photon-magnon interaction, YIG film is placed directly at one edge of the HRR. We examine the transmission spectra $|S_{21}|$ as a function of frequency by systematically varying the strength of the static magnetic field H_{dc} applied along the y -direction. This allowed us to investigate the individual behaviors of the HRR and YIG systems, as well as their collective behavior in the hybrid configuration. Initially, a simulation was conducted for the HRR without the YIG film, revealing the pure photon mode resonance frequency ω_c peak at 5.33 GHz in the $|S_{21}|$ spectrum with an associated damping constant of $\beta = \frac{\Delta\omega_{HWHM}}{\omega_c} = \frac{\kappa_c}{\omega_c}$ is 4.69×10^{-5} , where linewidth $\kappa_c/2\pi = 24.997\text{ MHz}$. The peak associated with the photon mode does not move with the H_{dc} (see supplementary materials). Also, the simulations were performed for the YIG film (i.e., without the ISRR), and the resonance frequency (ω_m) peak position varies with the magnitude of H_{dc} because the intrinsic precessional motion of magnetization depends on the strength of the applied field (see supplementary materials).

The frequency linewidth (HWHM) of YIG's magnon mode was estimated as $K_m = \Delta f/2$ and is related to the damping constant as $\alpha = K_m/\omega_m$. Subsequently, simulations including both the HRR and the YIG film were conducted in the presence of a static external magnetic field H_{dc} . Addition-

ally, to explore the impact of magnon dissipation rates on photon-magnon interactions, simulations were also conducted by varying the damping of the YIG film from 1.4×10^{-5} to 2.8×10^{-2} , achieved by controlling the ferromagnetic resonance linewidth (ΔH).

III. RESULTS AND DISCUSSIONS

Figure 2(a) shows the $|S_{21}|$ spectrum powers on the plane of $f - H_{dc}$ obtained for different damping parameters of YIG, in which the color variance indicates the intensity of the spectrum. Strong anti-crossing dispersion is observed for all α values, indicating the formation of upper and lower coupled branches near the resonant frequencies of the magnon and photon modes. This demonstrates robust coupling between the magnon mode of the YIG film and the photon mode of the HRR. However, the split-gap at the anti-crossing center becomes narrower with the increase in YIG damping, indicating a reduction in magnon-photon coupling strength.

This is accompanied by a broadening of the photon linewidth, as can be clearly evident from Fig. 2(b), representing the $|S_{21}|$ spectra as a function of frequency at the coupling center ($\omega_c = \omega_m$) for various values of α . The symbols (black), representing our simulation results, demon-

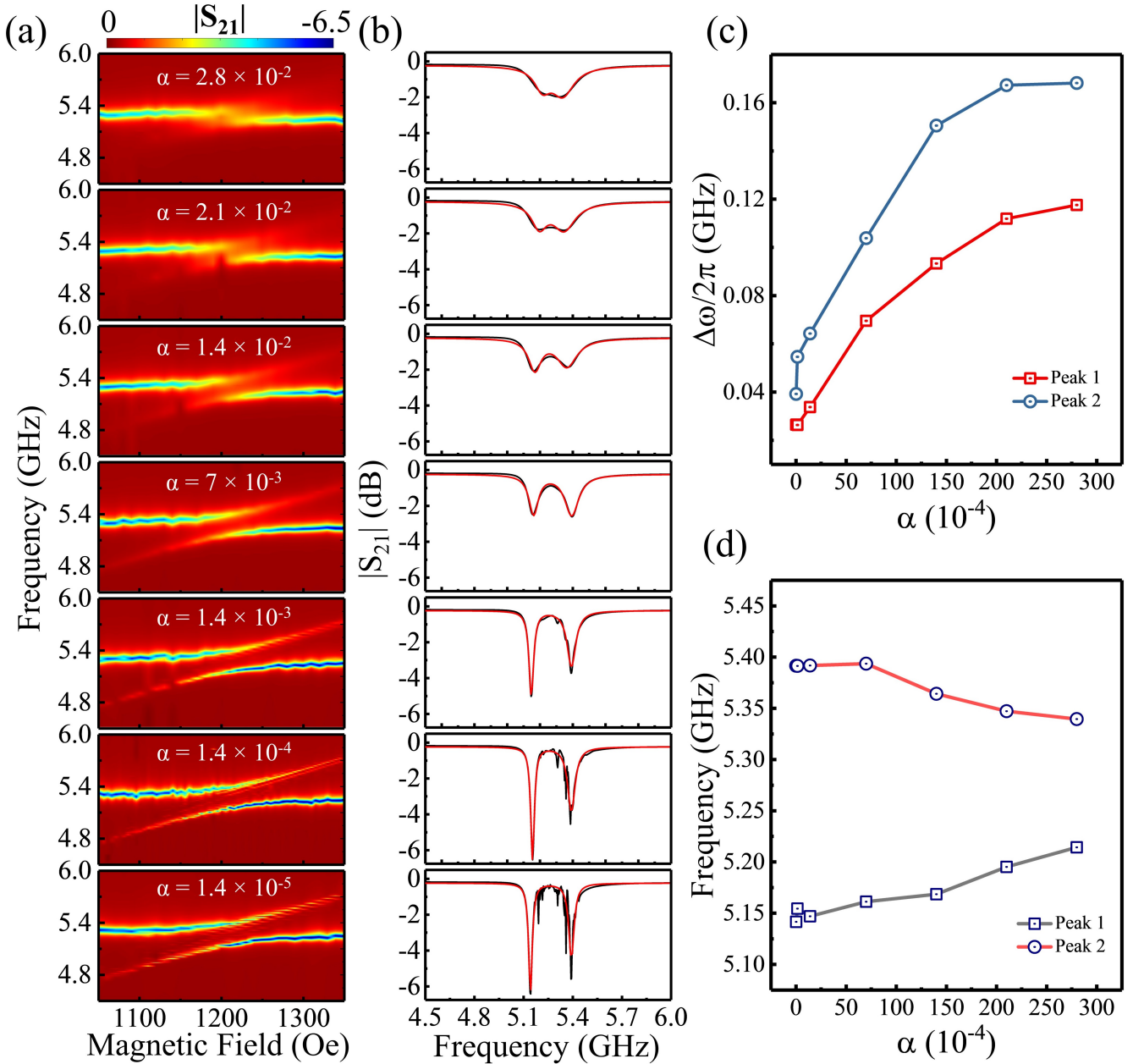


FIG. 2. From the simulation results: (a) The scanned $[f, H]$ dispersion of microwave $|S_{21}|$ power, showing a series of anti-crossing gaps simulated for various values of α . (b) The transmission spectra ($|S_{21}|$) as a function of microwave frequency at resonance ($\omega_c = \omega_m$) for different values of α , corresponding (c) linewidths of the peaks, and (d) the positions of the peaks.

strate that as α increases, the coupled split peaks progressively shift closer together, accompanied by a reduction in intensity. At $\alpha = 7 \times 10^{-3}$, the peaks begin to merge, and by $\alpha = 2.8 \times 10^{-2}$, they nearly coalesce into a single peak.

This is a direct manifestation of the reduction in magnon-photon coupling strength and the enhancement of photon damping as the damping of the YIG material increases, signaling increased photon dissipation and the onset of the Purcell effect. In this regime, photon dissipation dominates, and the system transitions to a Purcell regime where magnon mode dissipation plays a more prominent role in the interaction dy-

namics. The coupling strength varies depending on the competition between magnon damping and photon dissipation, as clearly evidenced in the spectra.

Our detailed analysis demonstrates that magnon damping plays a crucial role in controlling magnon-photon coupling strength and photon dissipation. The full-width at half-maximum ($\Delta\omega/2\pi$) and central frequencies of the split peaks, extracted from Fig. 2(b) and presented in Figs. 2(c) and 2(d), respectively, reveal a parabolic trend in FWHM and a convergence of the central frequencies with increasing magnon damping. The difference between the central frequencies de-

creases gradually at low magnon damping and significantly at higher damping.

To confirm the occurrence of the Purcell phenomenon, we analyze the coupling conditions within the coupling region. If the resonance frequencies exhibit anti-crossing and the linewidths cross at the coupling center, the coupling strength g must satisfy $(K_m - K_c)/2 < g \leq K_m$. On the other hand, if the dispersion shows crossing and the linewidths are anti-crossing, the condition becomes $(K_m - K_c)/2 \geq g > K_m$. Since, in our case, the dispersion spectra exhibit anti-crossing (see Fig. 2a), it is essential to satisfy the above Purcell condition that K_m must be greater than or equal to the coupling strength.

From Fig. 2(b), we extracted the gap between two peak positions for all values of α , which corresponds to the coupling strength between HRR and YIG. We found that the $K_m/2\pi$ exceeds the coupling strength $g/2\pi$ only for $\alpha = 2.1 \times 10^{-2}$ and 2.8×10^{-2} , where the corresponding values of $K_m/2\pi$ are 111.93 MHz and 149.24 MHz, and $g/2\pi$ are 76 MHz and 63 MHz, respectively. However, in the low damping region ($1.4 \times 10^{-5} \leq \alpha \leq 1.4 \times 10^{-2}$), $K_m/2\pi$ remains lower than the coupling strength (see Table 1).

Thus, we found that the parameters $K_m/2\pi$ and $g/2\pi$ only satisfy this condition for the two highest values of magnon damping. To confirm the Purcell effect for these two values of magnon damping, we need to determine the exact photon dissipation rate $K_c/2\pi$.

To quantitatively analyze the change in the photon dissipation rate ($K_c/2\pi$) and coupling strength of the PMC system, we construct a theoretical model based on the quantum harmonic oscillator. A schematic representation of the quantum model, consisting of a magnon mode (\hat{m}) in the YIG and a microwave photon mode (\hat{c}) in the HRR, is illustrated in Fig. 1(c). The magnon mode is coupled to the microwave photon mode via the microstrip feeding line, which facilitates the traveling wave interaction. The total Hamiltonian for the traveling wave-mediated PMC system is

$$H = H_0 + H_p + H_{\text{cmp}}, \quad (1a)$$

$$\begin{aligned} H = & \hbar\tilde{\omega}_c\hat{c}^\dagger\hat{c} + \hbar\tilde{\omega}_m\hat{m}^\dagger\hat{m} + \hbar g(\hat{c}^\dagger + \hat{c})(\hat{m}^\dagger + \hat{m}) \\ & + \hbar \int \omega_k \hat{p}_k^\dagger \hat{p}_k dk \\ & + \hbar \int \lambda_c (\hat{c} + \hat{c}^\dagger)(\hat{p}_k + \hat{p}_k^\dagger) dk \\ & + \hbar \int \lambda_m (\hat{m} + \hat{m}^\dagger)(\hat{p}_k + \hat{p}_k^\dagger) dk, \end{aligned} \quad (1b)$$

where H_0 is the magnon-photon Hamiltonian, which includes the kinetic terms for both the photon and magnon modes, along with all quadratic interactions. Here, \hat{c}^\dagger (\hat{c}) and \hat{m}^\dagger (\hat{m}) are the respective creation (annihilation) operators

of the photon and magnon modes, which have corresponding complex frequencies $\tilde{\omega}_c$ and $\tilde{\omega}_m$, respectively, and g is the coupling strength between the photon and magnon resonances. The Hamiltonian H_p for the traveling photon contains the kinetic term representing its propagation. Meanwhile, the Hamiltonian H_{cmp} describes the interaction of the traveling photon with the HRR's photon mode and the YIG's magnon mode, characterized by coupling strengths λ_c and λ_m , respectively. Here \hat{p}^\dagger (\hat{p}) is the creation (annihilation) operator for the traveling photon.

After applying the rotating wave approximation to Eq. 1 (see the Supplementary Materials), the total Hamiltonian H for the coupled system becomes:

$$\begin{aligned} H = & \hbar\tilde{\omega}_c\hat{c}^\dagger\hat{c} + \hbar\tilde{\omega}_m\hat{m}^\dagger\hat{m} + \hbar g(\hat{c}\hat{m}^\dagger + \hat{c}^\dagger\hat{m}) \\ & + \hbar \int \omega_k \hat{p}_k^\dagger \hat{p}_k dk \\ & + \hbar \int \lambda_c (\hat{c}\hat{p}_k^\dagger + \hat{c}^\dagger\hat{p}_k) dk \\ & \hbar \int \lambda_m (\hat{m}\hat{p}_k^\dagger + \hat{m}^\dagger\hat{p}_k) dk, \end{aligned} \quad (2)$$

Here, $\tilde{\omega}_c = \omega_c - i\beta\omega_c$, and $\tilde{\omega}_m = \omega_m - i\alpha\omega_m$, where β and α denote the intrinsic damping rates of the photon and magnon modes, respectively.

Using the commutation relation of the creation and annihilation operators $[\hat{c}_i, \hat{c}_j^\dagger] = \delta_{ij}$, and $[\hat{c}_i, \hat{c}_j] = [\hat{c}_i^\dagger, \hat{c}_j^\dagger] = 0$, the equation of motion for the photon and magnon modes can be written as:

$$\frac{d}{dt} \begin{bmatrix} \hat{c} \\ \hat{m} \end{bmatrix} = -i \begin{bmatrix} \tilde{\omega}_c - \lambda_c & g + i\sqrt{\lambda_c\lambda_m} \\ g + i\sqrt{\lambda_c\lambda_m} & \tilde{\omega}_m - \lambda_m \end{bmatrix} \begin{bmatrix} \hat{c} \\ \hat{m} \end{bmatrix} - i \begin{bmatrix} \sqrt{\lambda_c} \\ \sqrt{\lambda_m} \end{bmatrix} P_{\text{in}}(t). \quad (3a)$$

$$\frac{d}{dt} \begin{bmatrix} \hat{c} \\ \hat{m} \end{bmatrix} = -iH_{\text{eff}} \begin{bmatrix} \hat{c} \\ \hat{m} \end{bmatrix} - i \begin{bmatrix} \sqrt{\lambda_c} \\ \sqrt{\lambda_m} \end{bmatrix} P_{\text{in}}(t). \quad (3b)$$

Simplifying, the effective Hamiltonian for the coupled system becomes:

$$H_{\text{eff}} = \begin{bmatrix} \tilde{\omega}_c - \lambda_c & g + i\sqrt{\lambda_c\lambda_m} \\ g + i\sqrt{\lambda_c\lambda_m} & \tilde{\omega}_m - \lambda_m \end{bmatrix} = \begin{bmatrix} \tilde{\omega}'_c & g' \\ g' & \tilde{\omega}'_m \end{bmatrix}, \quad (4)$$

where $\tilde{\omega}'_c = \tilde{\omega}_c - \lambda_c$, $\tilde{\omega}'_m = \tilde{\omega}_m - \lambda_m$, and $g' = g - i\sqrt{\lambda_c\lambda_m}$. The eigenvalues of the coupling matrix can be expressed as:

$$\tilde{\omega}_\pm = \frac{1}{2} \left[\tilde{\omega}'_c + \tilde{\omega}'_m \pm \sqrt{(\tilde{\omega}'_c - \tilde{\omega}'_m)^2 + 4g'^2} \right]. \quad (5)$$

The transmission coefficient ($|S_{21}|$ spectra) for the PMC system, derived from Eq. 1 using input-output theory^{35,39}, is given by:

$$|S_{21}| = \frac{2\alpha\gamma_c\omega_m + 2\beta\gamma_m\omega_c - 4ig\sqrt{\gamma_c\gamma_m} - 2i\gamma_c(\omega - \omega_m) - 2i\gamma_m(\omega - \omega_c)}{[(ig + \sqrt{\gamma_c\gamma_m})^2 + (i\beta\omega_c + i\gamma_c + \omega - \omega_c)(i\alpha\omega_m + i\gamma_m + \omega - \omega_m)]}. \quad (6)$$

Here, $\gamma_{c,m} = 2\pi\lambda_{c,m}^2$, representing the extrinsic damping rates of HRR and YIG, respectively.

Using Eq. 6, we plotted the $|S_{21}|$ power as a function of frequency for different magnon damping values, as shown in Fig. 3(a). The variation in $|S_{21}|$ power with magnon damping closely aligns with our simulation results depicted in Fig. 2(a), demonstrating excellent agreement between the theoretical model and simulation. We also calculated the photon mode linewidth ($K_c/2\pi$) corresponding to magnon damping using our quantum model. From the calculated parameters ($K_c/2\pi$), ($g/2\pi$), and ($K_m/2\pi$) as listed in Table 1, we found that the Purcell condition, $((K_m - K_c)/2 < g \leq K_m)$, is satisfied only for $\alpha \geq 2.1 \times 10^{-2}$. The corresponding values of $K_c/2\pi$ are 39 MHz and 45.5 MHz, while $g/2\pi$ are 76.03 MHz and 62.6 MHz, respectively.

This result confirms the occurrence of the Purcell effect at higher magnon damping, further validating the accuracy and consistency of our theoretical model.

To further investigate the variation of coupling strength with magnon damping through quantum calculations, we calculated the coupling strength using Eq. (5) and presented the results as blue stars in Fig. 3(b). The analysis shows that the coupling strength decreases gradually for low magnon damping, reaching 116.61 MHz, but exhibits a pronounced reduction at higher damping, dropping to 62.6 MHz for $\alpha = 2.8 \times 10^{-2}$. The photon damping rate, calculated using Eq. (5) (see Table 1) and shown in Fig. 3(c), increases significantly with higher magnon damping and exhibits enhanced spontaneous emission only for $\alpha \geq 2.1 \times 10^{-2}$.

Furthermore, for the highest magnon damping ($\alpha = 2.8 \times 10^{-2}$), we calculated the FFT of the transmission spectra for two bias magnetic fields, $H_{dc1} = 900$ Oe and $H_{dc2} = 1210$ Oe, and plotted $|S_{21}|$ vs. time in Fig. 3(d). The figure demonstrates the enhanced photon decay rate at the coupling center (i.e., H_{dc2}) compared to an uncoupled state (i.e., H_{dc1}). For a clearer comparison, the transmission spectra for HRR alone and HRR+YIG are shown in Fig. 3(e). This figure highlights the increase in HRR linewidth from 24.99 MHz to 45.5 MHz due to the Purcell effect. These findings provide a comprehensive understanding of the system's transition into the Purcell regime.

IV. CONCLUSION

In summary, through numerical simulations, we systematically analyze the role of magnon damping in tailoring the coupled mode dynamics of a photon-magnon hybrid system. By varying the magnon damping, we identify the conditions for the emergence of the Purcell effect, characterized by reduced coupling strength and increased photon dissipation. Our quan-

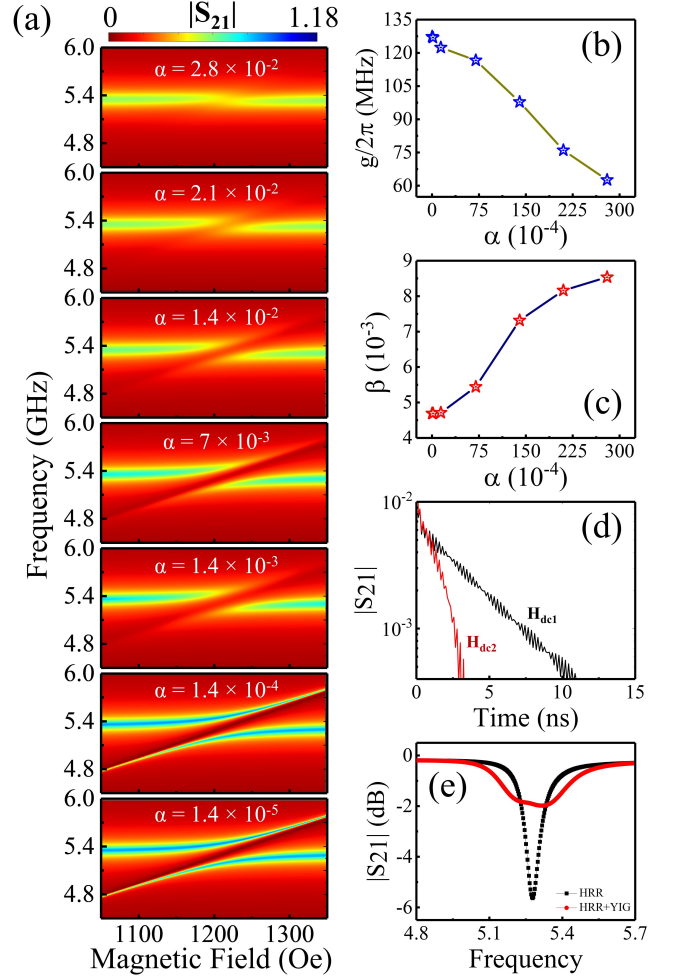


FIG. 3. (a) $|S_{21}|$ power of photon-magnon coupled modes on f-H plane, calculated using a quantum model for different values of magnon damping. The variation of (b) coupling strength ($g/2\pi$), and (c) the damping constant of the photon mode (β), both as functions of magnon damping (α). (d) The $|S_{21}|$ transmission Spectra as a function of time, are calculated using the FFT of simulation data; and (e) The $|S_{21}|$ spectra as a function of frequency, for two different bias magnetic fields ($H_{dc1} = 900$ Oe, and $H_{dc2} = 1210$ Oe) applied along the Y-direction, shown only for the highest magnon damping ($\alpha = 2.8 \times 10^{-2}$).

tum theoretical model findings not only validate the occurrence of the Purcell effect but also reveal new insights into the tunability of hybrid systems by manipulating dissipation channels. This study expands the scope of cavity magnonics, offering a novel pathway to dynamically control hybrid quantum systems for applications in quantum information science and beyond.

Sr. No.	α (10^{-4})	$K_m/2\pi$ (MHz)	$K_c/2\pi$ (MHz)	$g/2\pi$ (MHz)	β (10^{-3})	$(K_m - K_c)/2 < g \leq K_m$
1	0.14	0.07462	24.99	127.3	4.688	No
2	1.4	0.7462	24.997	126.9	4.7	No
3	14	7.462	25.15	122.38	4.718	No
4	70	37.31	29	116.61	5.44	No
5	140	74.62	39	97.82	7.317	No
6	210	111.93	43.5	76.03	8.161	Yes
7	280	149.24	45.5	62.6	8.536	Yes

TABLE I. Comparison of the Purcell Condition for different values of magnon damping (α), based on the frequency linewidth (HWHM) of magnon mode (K_m), frequency linewidth of photon mode (K_c), coupling strength (g), and damping constant of photon mode (β).

ACKNOWLEDGMENTS

The work was supported by the Council of Science and Technology, Uttar Pradesh (CSTUP), (Project Id: 2470, CST, U.P. sanction No: CST/D-1520). B. Bhoi acknowledges support by the Science and Engineering Research Board (SERB) India- SRG/2023/001355. R. Singh acknowledges support from the Council of Science and Technology, Uttar Pradesh (CSTUP), (Project Id: 4482). S. Verma acknowledges Ministry of Education, Government of India for the Prime Minister's Research Fellowship (PMRF ID-1102628).

DATA AVAILABILITY STATEMENT

The data that support the findings of this study are available within the article.

REFERENCES

- ¹M. Wallquist, K. Hammerer, P. Rabl, M. Lukin, and P. Zoller, "Hybrid quantum devices and quantum engineering," in *Physica Scripta T*, Vol. T137 (2009).
- ²G. Kurizki, P. Bertet, Y. Kubo, K. Mølmer, D. Petrosyan, P. Rabl, and J. Schmiedmayer, "Quantum technologies with hybrid systems," (2015).
- ³M. Harder, "Cavity spintronics foundations and applications of spin-photon hybridization by cavity spintronics by," PhD. Thesis (2018).
- ⁴D. DiVincenzo, "Book review on "quantum computation and quantum information (m nielsen/i chung)," Quantum Information and Computation **1** (2001), 10.26421/qic1.2-5.
- ⁵M. A. Nielsen and I. L. Chuang, *Quantum computation and quantum information* (Cambridge university press, 2010).
- ⁶J. Gollwitzer, L. Bocklage, R. Röhlberger, and G. Meier, "Connecting fano interference and the jaynes-cummings model in cavity magnonics," npj Quantum Information **7** (2021), 10.1038/s41534-021-00445-8.
- ⁷L. D. Stanfield, A. W. Powell, S. A. Horsley, J. R. Sambles, and A. P. Hibbins, "Microwave demonstration of purcell effect enhanced radiation efficiency," Scientific Reports **13** (2023), 10.1038/s41598-023-32066-w.
- ⁸A. Auffèves-Garnier, C. Simon, J.-M. Gérard, and J.-P. Poizat, "Giant optical nonlinearity induced by a single two-level system interacting with a cavity in the purcell regime," Phys. Rev. A **75**, 053823 (2007).
- ⁹A. E. Krasnok, A. P. Slobozhanyuk, C. R. Simovski, S. A. Tretyakov, A. N. Poddubny, A. E. Miroschnichenko, Y. S. Kivshar, and P. A. Belov, "An antenna model for the purcell effect," Scientific Reports **5** (2015), 10.1038/srep12956.
- ¹⁰Y. Zhao, L. Wang, X. Han, Y. Tian, S. Yan, Q. Guo, Y. Zhai, and L. Bai, "Control of magnon-photon coupling by a direct current in a py/pt-superconducting cavity hybrid system," Applied Physics Letters **122** (2023), 10.1063/5.0153616.
- ¹¹A. D. Gartman, A. S. Shorokhov, and A. A. Fedyanin, "Efficient light coupling and purcell effect enhancement for interlayer exciton emitters in 2d heterostructures combined with sin nanoparticles," Nanomaterials **13** (2023), 10.3390/nano13121821.
- ¹²M. Jordan, P. Androvitsaneas, R. N. Clark, A. Trapalis, I. Farrer, W. Langbein, and A. J. Bennett, "Probing purcell enhancement and photon collection efficiency of inas quantum dots at nodes of the cavity electric field," Physical Review Research **6** (2024), 10.1103/PhysRevResearch.6.L022004.
- ¹³B. Romeira and A. Fiore, "Purcell effect in the stimulated and spontaneous emission rates of nanoscale semiconductor lasers," (2018), 10.1109/JQE.2018.2802464.
- ¹⁴H. P. Adl, S. Gorji, M. K. Habil, I. Suárez, V. S. Chirvony, A. F. Gualdrón-Reyes, I. Mora-Seró, L. M. Valencia, M. D. L. Mata, J. Hernández-Saz, S. I. Molina, C. J. Zapata-Rodríguez, and J. P. Martínez-Pastor, "Purcell enhancement and wavelength shift of emitted light by cspbi3perovskite nanocrystals coupled to hyperbolic metamaterials," ACS Photonics **7**, 3152–3160 (2020).
- ¹⁵G. S. Agarwal, "Control of the purcell effect via unexcited atoms and exceptional points," Physical Review Research **6** (2024), 10.1103/PhysRevResearch.6.L012050.
- ¹⁶Z. Chen, J. Rao, K. X. Zhao, F. Yang, C. X. Wang, B. Yao, and W. Lu, "Manipulating the nonreciprocal microwave transmission by using a pump-induced magnon mode," Applied Physics Letters **125** (2024), 10.1063/5.0189615.
- ¹⁷Z. Qian, L. Shan, X. Zhang, Q. Liu, Y. Ma, Q. Gong, and Y. Gu, "Spontaneous emission in micro- or nanophotonic structures," (2021).
- ¹⁸X. Zhang, C. L. Zou, L. Jiang, and H. X. Tang, "Strongly coupled magnons and cavity microwave photons," Physical Review Letters **113** (2014), 10.1103/PhysRevLett.113.156401.
- ¹⁹C. Gou, X. Hu, J. Xu, and F. Wang, "Hybrid magnon-photon bundle emission from a ferromagnetic-superconducting system," Physical Review Research **6** (2024), 10.1103/PhysRevResearch.6.023052.
- ²⁰G. Zhao and X. Qian, "Magnonic purcell effect in a cavity system," in *Frontiers in Optics + Laser Science 2023 (FiO, LS)* (Optica Publishing Group, 2023) p. JTU5A.66.
- ²¹A. David, H. Benisty, and C. Weisbuch, "Photonic crystal light-emitting sources," Reports on Progress in Physics **75**, 126501 (2012).
- ²²M. Notomi, "Manipulating light with strongly modulated photonic crystals," Reports on Progress in Physics **73**, 096501 (2010).
- ²³Y. Akahane, T. Asano, B.-S. Song, and S. Noda, "High-q photonic nanocavity in a two-dimensional photonic crystal," Nature **425**, 944–947 (2003).
- ²⁴T. Asano, B.-S. Song, and S. Noda, "Analysis of the experimental q factors (> 1 million) of photonic crystal nanocavities," Optics Express **14**, 1996 (2006).
- ²⁵T. J. Kippenberg, S. M. Spillane, and K. J. Vahala, "Demonstration of ultra-high-q small mode volume toroid microcavities on a chip," Applied Physics Letters **85**, 6113–6115 (2004).
- ²⁶A. Kiraz, P. Michler, C. Becher, B. Gayral, A. Imamoğlu, L. Zhang, E. Hu, W. V. Schoenfeld, and P. M. Petroff, "Cavity-quantum electrodynamics using a single inas quantum dot in a microdisk structure," Applied Physics Letters **78**, 3932–3934 (2001).
- ²⁷K. J. Vahala, "Optical microcavities," Nature **424**, 839–846 (2003).

- ²⁸H. Thyrrstrup, L. Sapienza, and P. Lodahl, “Extraction of the β -factor for single quantum dots coupled to a photonic crystal waveguide,” *Applied Physics Letters* **96** (2010), 10.1063/1.3446873.
- ²⁹B. Zare Rameshti, S. Viola Kusminskiy, J. A. Haigh, K. Usami, D. Lachance-Quirion, Y. Nakamura, C.-M. Hu, H. X. Tang, G. E. Bauer, and Y. M. Blanter, “Cavity magnonics,” *Physics Reports* **979**, 1–61 (2022), cavity Magnonics.
- ³⁰B. Bhoi, B. Kim, S. H. Jang, J. Kim, J. Yang, Y. J. Cho, and S. K. Kim, “Abnormal anticrossing effect in photon-magnon coupling,” *Physical Review B* **99** (2019), 10.1103/PhysRevB.99.134426.
- ³¹B. Bhoi, B. Kim, J. Kim, Y. J. Cho, and S. K. Kim, “Robust magnon-photon coupling in a planar-geometry hybrid of inverted split-ring resonator and yig film,” *Scientific Reports* **7** (2017), 10.1038/s41598-017-12215-8.
- ³²S. Verma, A. Maurya, R. Singh, and B. Bhoi, “Control of photon-magnon coupling in a planar hybrid configuration,” *Journal of Superconductivity and Novel Magnetism* **37**, 1163–1171 (2024).
- ³³A. Maurya, K. K. Shrivastava, S. Verma, R. Singh, and B. Bhoi, “Room temperature photon-magnon coupling in yig- electric field coupled resonator system,” *Chemical Physics Impact* **9**, 100669 (2024).
- ³⁴A. A. Clerk, K. W. Lehnert, P. Bertet, J. R. Petta, and Y. Nakamura, “Hybrid quantum systems with circuit quantum electrodynamics,” (2020).
- ³⁵J. W. Rao, Y. P. Wang, Y. Yang, T. Yu, Y. S. Gui, X. L. Fan, D. S. Xue, and C.-M. Hu, “Interactions between a magnon mode and a cavity photon mode mediated by traveling photons,” *Physical Review B* **101**, 064404 (2020).
- ³⁶J. W. Rao, S. Kaur, B. M. Yao, E. R. Edwards, Y. T. Zhao, X. Fan, D. Xue, T. J. Silva, Y. S. Gui, and C. M. Hu, “Analogue of dynamic hall effect in cavity magnon polariton system and coherently controlled logic device,” *Nature Communications* **10** (2019), 10.1038/s41467-019-11021-2.
- ³⁷Z. Yang, Y. Li, J. Wang, Y. Zuo, T.-X. Lu, H. Jing, and C. Ren, “Microwave quantum illumination: enhanced azimuth detection with cavity magnonics,” *Optics Express* **32**, 28293 (2024).
- ³⁸P. Androvitsaneas, A. B. Young, C. Schneider, S. Maier, M. Kamp, S. Höfling, S. Knauer, E. Harbord, C. Y. Hu, J. G. Rarity, and R. Oulton, “Charged quantum dot micropillar system for deterministic light-matter interactions,” *Physical Review B* **93** (2016), 10.1103/PhysRevB.93.241409.
- ³⁹K. K. Shrivastava, A. Sahu, B. Bhoi, and R. Singh, “Unveiling photon–photon coupling induced transparency and absorption,” *Journal of Physics D: Applied Physics* **57**, 465305 (2024).